DEM Analysis and Prediction for the Lateral Interaction of Monopile in Gravel Soil

Wanquan Sun & Emile Niringiyimana

ONLINE FIRST

Geotechnical and Geological Engineering
An International Journal

ISSN 0960-3182

Geotech Geol Eng
DOI 10.1007/s10706-020-01406-2

Springer

Geotech Geol Eng
https://doi.org/10.1007/s10706-020-01406-2

ORIGINAL PAPER

DEM Analysis and Prediction for the Lateral Interaction of Monopile in Gravel Soil

Wanquan Sun · Emile Niringiyimana

Received: 4 December 2019 / Accepted: 4 June 2020

Abstract Gravel is a common geotechnical material in civil engineering. To investigate the lateral bearing behavior of monopile in gravel materials and deeply understand the microscopic mechanisms, parametric three-dimensional discrete element analyses are performed to study the lateral interaction between the single pile and gravel. First, using the experimental data of two typical gravel samples, the discrete element methods (DEM) for monopile in gravel materials are investigated. A discrete particle flow model of pile segments that allows for the construction of p–y curves at various depths is proposed. The lateral mechanical behaviors (p–y curves) between monopile and different gravel material are then studied. The effects of gravel porosity, distribution and grain-size on both the strength and shape of the p–y curves are investigated. The results show that the influences of porosity and depth on the p–y behaviors of gravel are significantly different from those of sand. Furthermore, the obvious differences in p–y behaviors between the coarse gravel and fine sand are the effects of grain size and size distribution. Based on these results, corresponding equations for the estimation of the p–y curves are proposed and further validated by independent field test data. It is concluded that the proposed p–y curve is capable of modeling both different grain sizes and size distributions in gravel-monopile interaction analyses during lateral loading.

Keywords Monopile · Gravel · p–y curve · Lateral loading · Discrete element method

W. Sun (✉) · E. Niringiyimana
Institute of Hydroelectric and Geotechnical Engineering, North China Electric Power University, Beijing 102206, China
e-mail: wqsun05@163.com

1 Introduction

Piles are often used for the foundation of bridges and hydropower engineering, and are constructed on sandy gravel or backfill gravel (Smith et al. 2000; Rollins et al. 2012; Chiou et al. 2012; Rollins et al. 2008). There are several different methods for estimating the complex soil-pile interactions, including the numerical analyzing methods (continuum, discontinuum and hybrid) (Azizkandi et al. 2018; Zhao et al. 2019; Haque and Abu-Farsakh 2019) and field loading test methods (Saeedi Azizkandi et al. 2014; Hamed et al. 2019), etc. Each method has its own advantages and disadvantages in context of soil resistance problems. In recent years, the popular approach for analyzing the lateral interaction between the pile and soil has been the subgrade reaction method, in which the pile is modeled as an elastic beam and the soil is modeled as nonlinear springs (defined as p–y curves). The nonlinear stiffness of each spring depends on factors including ultimate resistance, shear strength, pile diameter, and depth (API 2000). The major advantage

Published online: 10 June 2020

of the p–y method is the ability to calculate key features of pile-soil interaction with less computational effort (Mayoral et al. 2016).

Many criteria for p–y curves have been proposed for modeling different types of soils based on field experiments, small-scale model tests, or finite element analyses. Examples include p–y curves for soft clays (Matlock 1970) and stiff clays (Reese et al. 1975), p–y curves for sands (Reese et al. 1974), and p–y curves for weak rock (Reese 1997) and frozen soils (Li and Yang 2017). However, most empirical procedures for p–y curves of granular soil are derived from load tests in sand. There are relatively few lateral load tests, and very limited information is available for piles in gravelly soils.

Coarse gravel material and sand have different mechanical and physical proprieties, and react differently under internal and external loads. Macklin and Chou (1989) completed a lateral load test for seven-foot (2.1 m) diameter caissons (drilled shafts) of bridges. The gravel parameters were back-calculated from load deflection and inclinometer data using p–y analysis. Smith et al. (2000) defined p–y curves constructed from field pressuremeter data, which was derived from the site investigation into the subsurface gravels, sandy gravels, and near mudline silts. Rollins et al. (2011, 2012) investigated the reduced lateral resistance of abutment piles near MSE walls based on full-scale tests in gravelly soils, and back-analyses using a p–y curve approach found the friction angle and k value of gravelly soils. Chiou et al. (2012) carried out an in situ lateral load test on a caisson-type foundation with a high gravel content, and obtained the modified p–y curves for the test caisson.

Differing from the previous literatures which back-calculated the relevant gravel parameters from a field experiment or generated p–y values using the non-linear finite element approach, this paper presents a procedure for the modeling of laterally loaded piles in gravel using three-dimensional discrete particle flow code (PFC3D) in consideration of the gradation and grain shape of gravel. Much of the previous research was based on two-dimensional small scale models (Jenck et al. 2009; Omidvar et al. 2014; Lobo-Guerrero and Vallejo 2007), which could be obtained with few particles. However, the lateral behavior of pile socketed into gravelly soil differs from previous studies because the total lateral resistance includes two parts of soil reactions: the soil resistance in front of the pile and the side shear force (Chiou et al. 2012). In addition, two-dimensional models cannot simulate soil failures in a conical wedge that extends to the soil surface. If a full-scale, three-dimensional PFC model that includes the whole pile and gravelly soil was to be built, large populations of particles would be required, which would result in solution difficulty. Therefore, to derive the p–y curves of each spring, the authors have built a three-dimensional PFC model per unit length (or height) of pile-gravel interaction at a certain depth. Based on numerical simulations verified with experimental data, the p–y approach for gravel is proposed, and the p–y curves are obtained.

The outline of the article is as follows. In Sect. 2, two types of gravelly soils with different grain-size distributions are chosen. Their micromechanical parameters, including particle stiffness and friction coefficient, were obtained during the calibration process, and all subsequent particle flow simulations are based on these parameters. In Sect. 3, the approach for simulating the laterally loaded piles in gravel using PFC3D is described. Based on the discrete numerical model of pile-gravel, the p–y curves for gravel material are obtained. The differences of these p–y curves obtained from many types of grain compositions of gravel materials are investigated, and the effects of granular porosity, gravel distribution, and grain size on the gravelly soil response of a pile subjected to lateral loads are also respectively studied. In Sect. 4, based on the previous analysis, the corresponding p–y equations for gravel material are ultimately derived, and are also validated by independent field testing data. The important factors that affect the lateral resistance of gravel for single piles, including porosity, grain size, and size distribution, are reasonably considered in the proposed equations.

2 Discrete Particle Simulation of Gravel

Due to limitations of the classical continuum approaches (FEM), particle-based methods like PFC3D are an alternative to the often very complex and complicated to handle elasto-plastic or hypo-plastic approaches used in continuum mechanical methods. PFC3D models the movement and interaction of spherical particles by the discrete element method (DEM), as described by PFC User's Guide (2008). It is also possible to create particles of arbitrary shape by attaching two or more particles together. Calculation method with PFC3D is a time-stepping, explicit scheme, which involves the execution of many thousands of time steps. At each step, Newton's second law (force = mass × acceleration) is integrated twice for each particle to provide updated velocities and new positions, given a set of contact forces acting on the particle. Based on these new particle positions, contact forces are derived from the relative displacements of pairs of particles; a linear or nonlinear force/displacement law at contacts may be used.

2.1 Brief Description of Selected Gravel and Experiments

The gravel samples were selected for the investigation, which have to fulfill the following requirements: (1) Samples can represent typical grain-size distributions of gravels, including well-graded and poorly-graded. (2) Since the computational time is governed both by the number of particles and the size of the smallest particle, it was necessary to select suitable grain-size distributions in consideration of the computational capabilities. (3) Adequate laboratory or field experiment data for calibration micromechanical parameters purposes.

Based on the mentioned requirements, two kinds of gravels, which were selected from lab test materials, were modeled in this study. Details of the test site, instrumentation, test method, mechanical properties of gravel, and other data can be found in Stahl and Konietzky (2011). A brief summary is subsequently provided.

The following two types of lab samples with different grain-size distributions were chosen for the numerical simulation study by Stahl.

Sample1 = gravel with a grain-size distribution of 12.5/16 mm (**abbr. 126**)

Sample2 = gravel with a grain-size distribution of 5/32 mm (**abbr. 532**)

In this paper, the results of lab tests described in the literature were utilized for the calibration of the micromechanical parameters of succeeding pile-gravel models.

2.2 Calibration of Micromechanical Parameters

PFC3D (2008) simulates a pile-gravelly soil system comprised of rigid spherical particles and walls for the purposes of compaction and confinement. Although gravel materials may exhibit complex nonlinear constitutive behavior, this can be achieved through the use of relatively simple contact models in PFC3D. The linear contact model used in this study is defined by the normal stiffness (k_n) and shear stiffness (k_s) of two adjacent entities. If the two particles have the same normal stiffness and shear stiffness, the relation between these stiffnesses and the modulus at a single contact is obtained by PFC3D (2008).

$$k_n = k_s = 4\bar{E}R, \tag{1}$$

where $\bar{E}$ is the apparent Young's modulus and R is the particle radii. It is obvious that the values of k_n and k_s greatly influence the initial stiffness modulus of gravelly soils.

The slip between two balls or between a ball and a wall is described in terms of a friction coefficient (f) that limits the shear force at contact. Because the gravelly soil is non-bonding, the parameters that determine the material peak strength are the friction coefficient and porosity. Under no-gravity conditions for the simulation of gravelly soil by particles in PFC, certain porosity can be achieved by the loading of boundaries (walls).

Based on the preceding analysis, the reasonable values of the micro-parameters (k_n, k_s, and f) can be obtained by a series of calibrating tests, and all the upcoming numerical tests will be based on these parameters.

The calibration process consists of the following steps: The normal-stiffness (k_n) and shear-stiffness (k_s) of Sample 1 and 2 are calibrated by comparing the initial moduli of the triaxial tests in Stahl and Konietzky (2011) with the numerical simulations results using the particles in PFC^{3D}. Figure 1 shows the representative characteristic curves in calibration procedure. The friction coefficients of sample 1 and 2 are calibrated in terms of ultimate strengths of the triaxial tests at different confining stresses. The change in porosity is very small with the change of confining stress, and its change happens in the third decimal place.

The results of the calibrated micro-parameters are summarized in Table 1. It should be noted that the

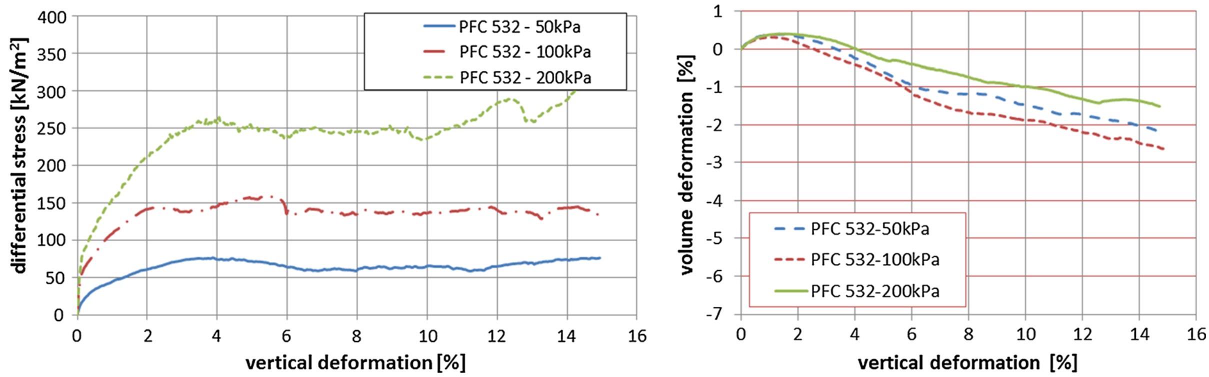

Fig. 1 Stress–strain and volume deformation behaviors of the calibration tests (soil 532) using different confining stresses

Table 1 Micromechanical parameters for soil 126 and 532 resulting from calibration tests

Gravel	Friction coefficient	Different loading conditions	Stiffnesses k_n and k_s (N/m)	Porosity	
				PFC	Lab or Field test
126	0.25	Confining stress of 50 kPa	4.0×10^5	0.436	0.42
		100 kPa	1.0×10^6	0.434	
532	0.24	Confining stress of 50 kPa	6.0×10^5	0.408	0.38
		100 kPa	1.4×10^6	0.407	
		200 kPa	2.2×10^6	0.405	

micro-parameters are the equivalent stiffness values for PFC3D particles simulating gravel material. Figure 1 presents the stress–strain responses and volumetric responses based on the calibrated micro-parameters, which coincide well with the results of lab tests.

The contact stiffnesses k_n and k_s (or the Young's modulus) vary with confining pressure at different depths, as shown in Eq. (2) (Fan and Long 2005; Jagodnik and Arbanas 2015).

$$k = k_0\left(\frac{p}{p_a}\right)^a \quad \text{or} \quad E = E_0\left(\frac{p}{p_a}\right)^a, \tag{2}$$

where p is the effective mean normal stress at a certain depth, E_0 is Young's modulus, p_a is atmospheric pressure, and a is constant for a given void ratio. In this work, a can be obtained by fitting using the calibrated stiffness. For example, the values of a for soil 126 and soil 532 at a pressure of 100 kPa are 1.33 and 1.23, respectively.

3 Study of the p–y Curves for Gravelly Soils

In this paper, an analytical method of the pile-gravelly soil lateral interaction is developed to consider the non-linear horizontal spring. The non-linear behavior of each spring, defined as the ''p–y curve'' depends on several factors including gravel type, shear strength, deformation characteristics, spring depth, and pile diameter. The p–y curves of each spring can be established directly in terms of gravel lateral resistance per unit length of the pile at different depths.

3.1 PFC3D Modeling of Laterally Loaded Pile Socketed into Gravelly Soil

The method of building the three-dimensional PFC model is presented in Fig. 2. The tests were carried out on gravelly soils with a dry density of 2.6×10^3 kg/m^3 and a pile with a diameter of 0.25 m and depth of 5 m. According to the results in Yu et al. (2019), the soil's horizontal influential range is 1.75D behind the pile, 2.45D ahead of the pile, and only 1.1D at the sides

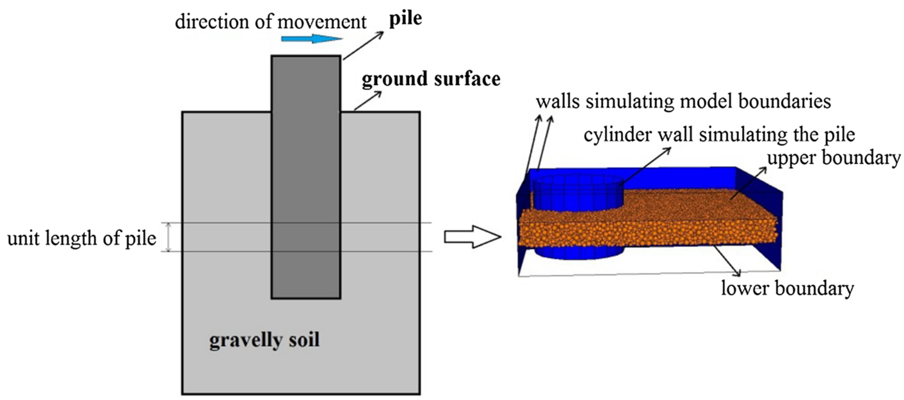

Fig. 2 Building the PFC model for pile-gravel lateral interaction at a certain depth

of the pile. In this study, thus, the model boundary in front of the pile was 4.8 times pile diameters (1.2 m). The boundary on both sides of the pile was 2.8 times pile diameters (0.7 m) as shown in Fig. 6. These model heights of pile segments were uniform at 0.2 m (i.e., the unit length of the pile at a certain depth, as shown in Fig. 2).

Walls were used in this study both to define boundary constraints of the model and to assist with the generation and compaction of balls. The micromechanical parameters (f, k_n, and k_s) of the surrounding walls have the same values as the particles that were calibrated in Sect. 2. The friction coefficients (f) of the upper boundary and lower boundary walls were set to zero due to the vertical symmetry. The influence of different soil depths can be simulated by changing the pressure of the upper boundary wall. For example, the pressure of the upper boundary wall of the 3-m-depth model is equal to the previous calibrated wall pressure at 1-m depth plus the 2-m soil gravity, etc. Therefore, this model can reliably account for the nonlinear pile-gravelly soil lateral interaction at different depths while still allowing for detailed gravelly soil modeling with limited computational effort. However, the method ignores the bending deformation of the pile per unit length at a certain depth, which has little influence on the lateral resistance of the long pile or the short pile with smaller displacement.

3.2 P–y Curves of Different Gravelly Soils

The main objective of this study is to provide insight into the effect of different gravelly soils on the p–y curves and to construct corresponding p–y equations for gravelly soils. Therefore, a series of numerical simulation tests was conducted on the pile-gravel lateral interaction, including different gravel porosities, gradations, and different grain sizes.

3.2.1 Effects of the Gravel Size Distribution and Porosity

Soil 126 and soil 532 with different porosities (10, 20, 30, and 35%) were chosen for tests. The different porosities were created by generating different amounts of particles in a uniform region. The results of the computed p–y curves are presented in Figs. 3, 4, and 5, and illustrate the evolution of the initial modulus of the subgrade reaction (K) and ultimate resistance (p_u) against the porosities of soil 532 and soil 126, respectively. The microscopic contact forces near the pile are shown in Fig. 6.

The results of these tests indicate that the p–y curves obviously changed depending on the porosity of the gravel and the sand. The K and p_u values vary linearly with the porosity. When the porosity

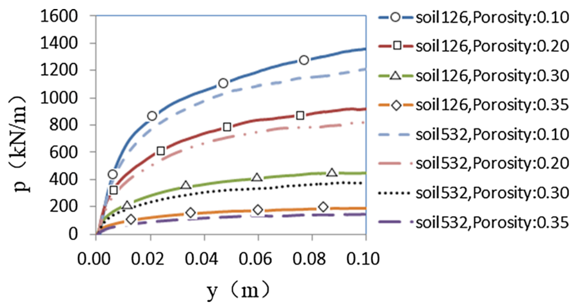

Fig. 3 The p–y curves of the different grain-size distributions and porosities

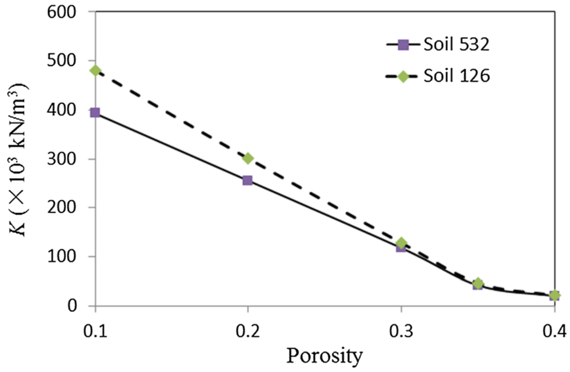

Fig. 4 Evolution of the initial modulus of subgrade reaction (K) against porosity

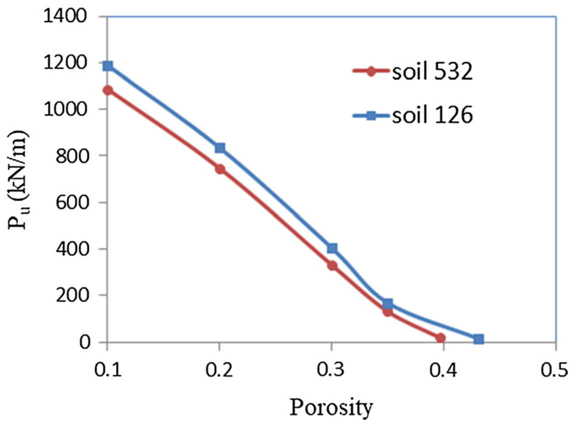

Fig. 5 Evolution of the ultimate resistance (p_u) against porosity

decreases by 10%, the values of K and p_u will approximately increase by 150 kN/m^3 and 400 kN/m, respectively.

The results show that under the condition of the same porosity, the gravel resistances (p) of soil 126 are higher than those of soil 532. As the porosity decreases (or compactness increases), the difference of gravel resistance between the two types of gravels will be larger. The primary reason for the difference is that there are many free smaller particles in the inner area of the relatively inhomogeneous soil 532. These smaller particles mixed in with the larger particles cannot provide effective contact forces. Figure 6 shows snapshots of the microscopic contact force network for soil 532 and soil 126. Each contact force is represented by a line segment that connects the centroids of two contact particles, and the width of the lines is proportional to the contact force. Obviously, the coarse particles often capture the largest force chains, whereas the fine particles often capture relatively small force chains. The gravel mixtures therefore became more non-homogenous in their force transmission as the gravels diameter difference increased. Specifically, fine particles were easily trapped in the voids of the skeleton of coarse particles in soil 532, which caused potential instability fabrics. On the other hand, the anisotropies of gravel materials are also the essential origins of resistance. The difference between the gravel resistances of soil 532 and soil 126 was attributed to the differences in the anisotropies of force chain distribution. A detailed analysis on the anisotropies of binary mixtures can be found in Gong and Liu (2017). However, in nature or in the actual project, the inhomogeneous gravelly soil (soil 532) usually has smaller porosity than homogeneous gravelly soils (soil 126), so the inhomogeneous gravelly soil will generate larger lateral resistance. The analysis is similar to the results of the lab triaxial tests conducted by Stahl and Konietzky (2011).

In addition, at the same porosity, the distribution of gravels (i.e., the percentages by weight of coarse gravels and fine gravels) may have many forms. Many researchers determined that the percentage by weight of coarse gravels, W, significantly affects the mechanical behavior of gravels. Therefore, the gravel resistance to pile will be affected by the distribution of gravels as well. For further study of the gravel resistance, refer to the experimental results of granular mixtures in Vallejo (2001) and Ueda et al. (2011). Figure 7 displays the variation in relative peak friction angle (ϕ_p/ϕ_{pW0}) of the binary mixtures (coarse particles and fine particles) as a function of W, where ϕ_p denotes the peak friction angle of binary mixtures, and ϕ_{pW0} denotes the peak friction angle of pure fine particles. Clearly, the values of relative friction angle barely change with increasing coarse particle content for W $\leq$ 30–40%. The peak friction angle monotonously increases with increasing W for W $>$ 40%. In addition, a slight decrease in peak friction angle was observed when W varied from 90 to 100%.

3.2.2 *Effects of Grain Size*

To construct the p–y equations, the influence of grain size on the lateral gravelly soil resistance must be studied independently under the condition of the same porosity; the effects of porosity have been excluded in the present study. Accordingly, more simulations were

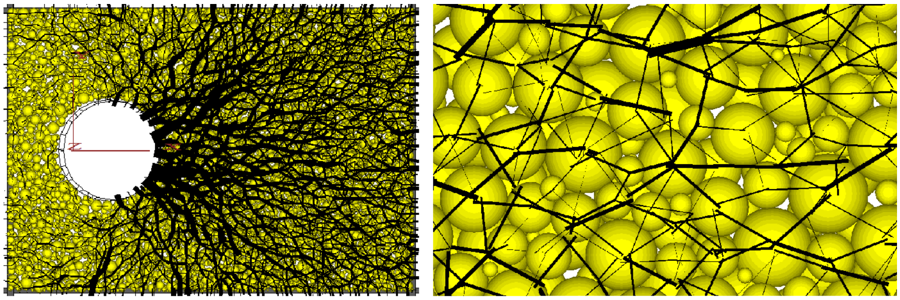

(a) soil 532

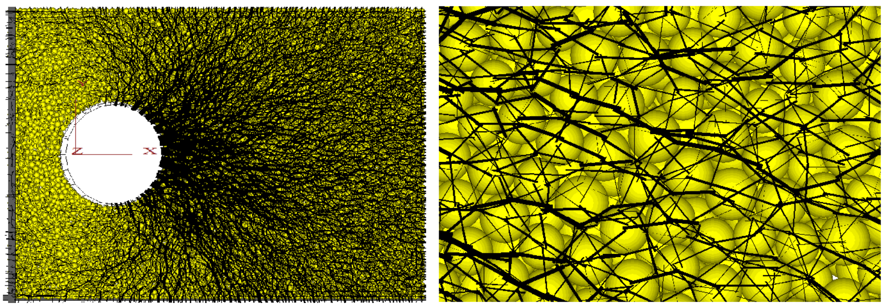

(b) soil 126

Fig. 6 Different magnifications of microscopic contact forces in the pile-gravel lateral interaction

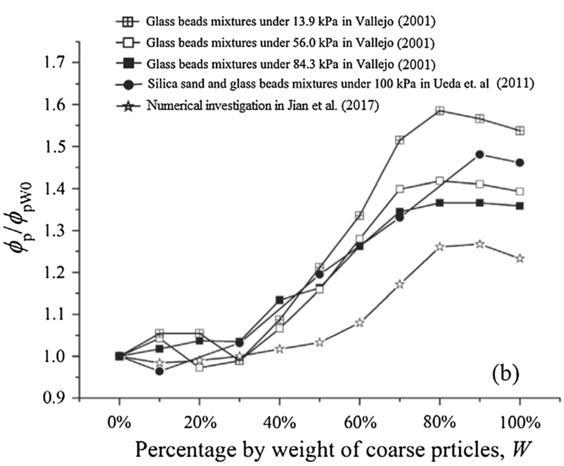

Fig. 7 The evolutions of the relative peak friction angle (ϕ_p/ϕ_{pW0}) against W (Gong and Liu 2017)

performed to calculate the p–y curves for different grain sizes of gravel. According to the calibrated micromechanical parameters in Sect. 2.2, the porosity of the free dropped gravel material is nearly 40%, so these model calculations were based on same porosities of 30 and 40%, which correspond to a relatively dense and loose compactness, respectively. These calculating cases include those in which the gravel size is 1–7 times that of gravel 126. The computed p–y curves are shown in Fig. 8, which indicates that when the porosity is the same, the grain sizes of gravelly soils have evident influence on the p–y performance of initial modulus of the reaction (K) and the ultimate resistance (p_u). For example, if the lateral resistance at a large pile displacement of 0.1 m is taken as the ultimate resistance, p_u, when the grain radii of soil 126 increase by 7 times, the K and p_u values corresponding to 30% porosity will increase by 1.45 and 1.8 times, respectively. In addition, as the grain sizes decrease, the gravel will tend to the ultimate lateral reaction p_u earlier. Some curves of numerical results show the fluctuation or decline trend (as shown at the end of "5 times size" curve). The phenomenon should be resulted in by the greater interlocking action and sudden energy release during the shearing and sliding process of gravel particles. The issues related to the size effects of gravel grains have been discussed previously by Ueda et al. (2011) and Salimi et al. (2008). Ueda et al. (2011) investigated the measured angle of shear resistance (φ) of binary mixtures of different grains sizes. As similar to the results in this

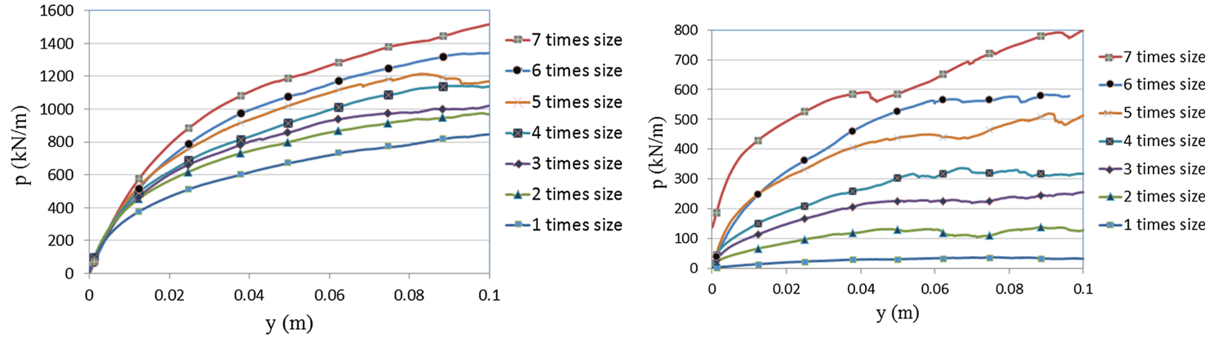

Fig. 8 Computed p–y curves of different gravel sizes with the same porosities

paper, the angle of shear resistance increases linearly with the increase of large particles content. With increasing the content of large particles from 30 to 90%, the shear strength of the sample will be increased by approximately 1.6 times. The study in Salimi et al. (2008) shows that the shear stress–shear displacement curves for samples with 60% gravel content. It indicates the shear strength will be increased by 1.28 times when the maximum grain size increases by 2 times.

By comparing the p–y curves obtained from 30% porosity (Fig. 8a) and those obtained from 40% (Fig. 8b) porosity, it was seen that the absolute variations of p values varied little with the size of gravel, but the relative variations of p values varied greatly between different gravel sizes. For example, the p_u value of 7 times size in 30% porosity is equal to 1.8 times that of 1 times size, however, the variation in 40% porosity will be 24 times. The results indicate that the relative variations of p values were more sensitive to the gravel size variation when the porosity was larger. The inner reason is clear and easy to understand, i.e., a low porosity implies dense packing and compacted state, the force chains between the smaller gravels will be more steady. Therefore, at low porosity, the mechanical behavior of several closely packed small gravels is closer to that of large size gravel, and the effect of gravel size on gravel resistance is relative smaller.

Based on the analysis of the variations of the K and p_u values with the grain size, a regression analysis on the data from numerical simulation research is conducted in this study. The fitting results are presented in Figs. 9 and 10 corresponding to 30% porosity and 40% porosity, respectively. The amplified coefficient β for K and amplified coefficient μ for p_u can be estimated as the empirical functions of the average grain size by the following:

When relatively dense packing (30% porosity),

$$\begin{cases} \beta = k * (\text{average grain size}) + 0.925 & \text{(3a)} \\ \mu = k' * (\text{average grain size}) + 0.867 & \text{(3b)} \end{cases}$$

where k is 0.00526 for homogeneous gravel and 0.00405 for inhomogeneous gravel. k' is 0.00935 for homogeneous gravel and 0.0072 for inhomogeneous gravel. The unit of average grain size is millimeters.

When relatively loose packing (40% porosity),

$$\begin{cases} \beta = k * (\text{average grain size}) - 4.778 & \text{(4a)} \\ \mu = k' * (\text{average grain size}) - 3.596 & \text{(4b)} \end{cases}$$

where k is 0.436 for homogeneous gravel and 0.336 for inhomogeneous gravel. k' is 0.263 for homogeneous gravel and 0.203 for inhomogeneous gravel. The unit of average grain size is millimeters.

3.2.3 *Effects of Depth*

Previous studies (API 2000; Stahl and Konietzky 2011) have concluded that the behavior of p–y curves is significantly affected by the depth. In fact, the influence of the depth is primarily caused by the soil confining pressure near the pile. Within a certain range of depth, the confining pressure of soil varies significantly, whereas the porosity basically remains stable. Figure 11 presents the comparison of the computed p–y curves at various depths for soil 532 and soil 126. Figures 12 and 13 illustrate the evolution of K and p_u per unit pile diameter against the depth, respectively.

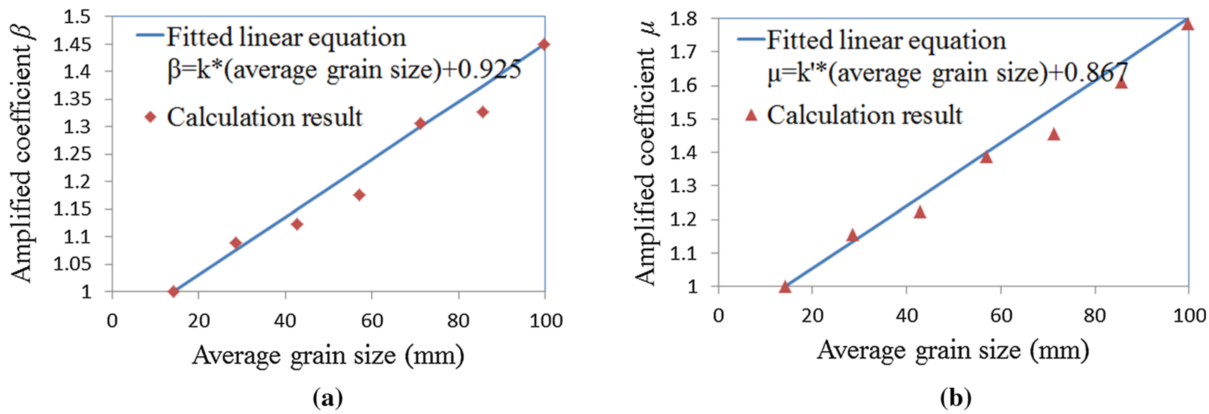

Fig. 9 Linear equations for predicting the amplified coefficients of initial subgrade reaction modulus (K) (**a**) and ultimate reaction (p_u) (**b**) for 30% porosity

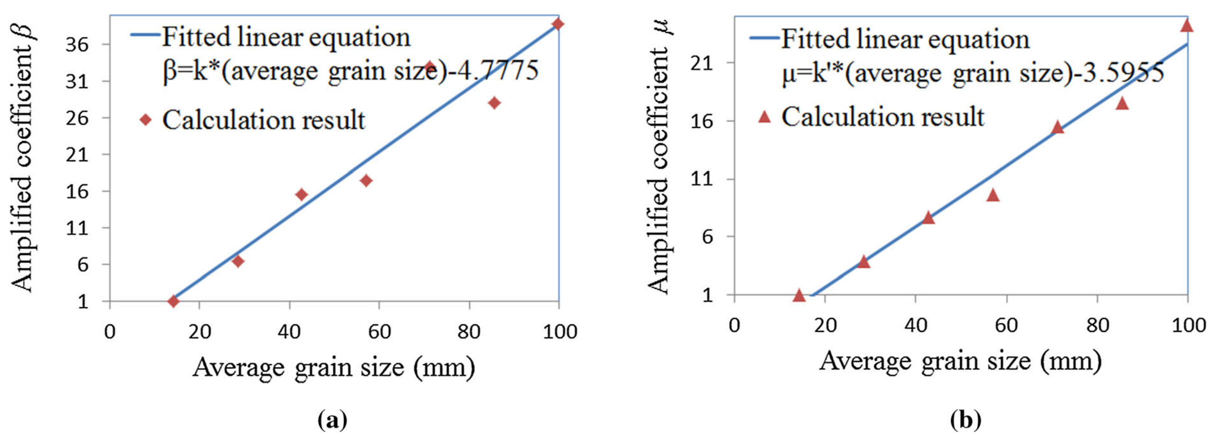

Fig. 10 Linear equations for predicting the amplified coefficients of initial subgrade reaction modulus (K) (**a**) and ultimate reaction (p_u) (**b**) for 40% porosity

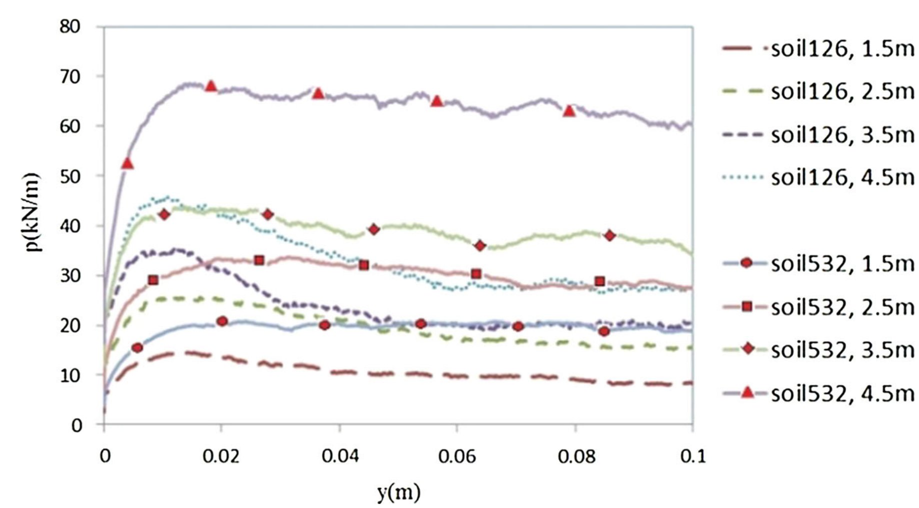

Fig. 11 Comparison of computed p–y curves at various depths for soil 532 with a porosity of 40% and soil 126 with a porosity of 43%

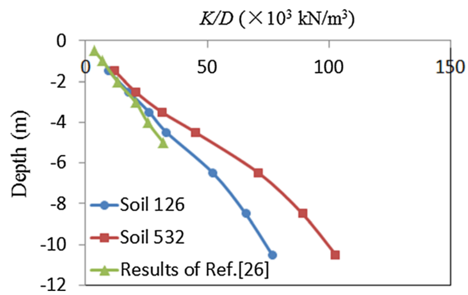

Fig. 12 Evolution of the initial modulus of the subgrade reaction (*K/D*, per unit pile diameter) against depth

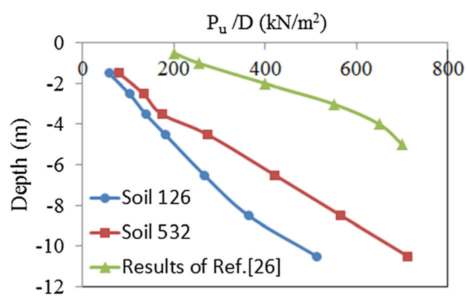

Fig. 13 Evolution of the ultimate resistance (p_u/D, per unit pile diameter) against depth

The results show that the lateral resistances (p) of soil 532 are higher than those of soil 126 at various depths. As the depth increases, the difference of lateral resistance between the two types of gravels will be larger. That is, the relative sensitivity of lateral resistance (p) to variations in depth for soil 532 is higher than that for soil 126, including the initial modulus of the reaction (K) and the ultimate resistance (p_u). The primary reason for this difference is that the porosity of the relatively inhomogeneous soil 532 is smaller and more sensitive than that of soil 126 in these tests.

Yu et al. (2019) studied the effect of cement-improved gravel soil on the bearing capacity of a single pile. Some typical back-analysis and fitted p–y curves at different depths (0.5–5.0 m) were obtained through field load tests and three-dimensional finite element analyses. Using the results in Yu et al. (2019), the corresponding K and p_u values per unit pile diameter against the depth is also displayed in Figs. 12 and 13. By comparing the curves in Figs. 12 and 13, it can be verified that the slope and the gradient of K and p_u as depths changes obtained from the PFC model are similar to that of Yu et al. (2019).

4 P–y Equations for Gravelly Soils

4.1 Constructing p–y Equations for Gravelly Soils

Previous studies have concluded that while the p–y behaviors of gravelly soils are somewhat similar to those of sand, the influences of porosity and depth on the p–y behaviors of gravel are significantly different from those of sand. Furthermore, the obvious differences between the p–y behaviors of gravel and sand are the effects of grain size and size distribution that should be considered in gravelly soils. Based on the preceding analysis and by referring to the p–y curves for sand (Azizkandi et al. 2018), the equations for p–y relationship curves are suggested by Eq. (5a):

$$P = p_u \times \tanh\left[\frac{\alpha \times \beta \times \varphi \times K \times H}{p_u} \times y\right], \tag{5a}$$

$$\varphi = 0.8232D + 0.7942, \tag{5b}$$

where D is the pile diameter (m), φ is the factor to account for the effect of D on K, K is the initial modulus of the subgrade reaction ($\times\ 10^3$ kN/m^3) and was determined from Fig. 4 as function of porosity. In addition, α is the factor to account for the variation of K with the depth of the different gravel size distributions (122 for inhomogeneous gravel and 116 for homogeneous gravel); α was derived through Fig. 12. β is the amplified coefficient for K considering the variation of grain size, and is defined in Eq. (3a) or Eq. (4a), H is depth (m), and p_u is the ultimate resistance of gravelly soils (kN/m) and can be derived through Eqs. (6–8).

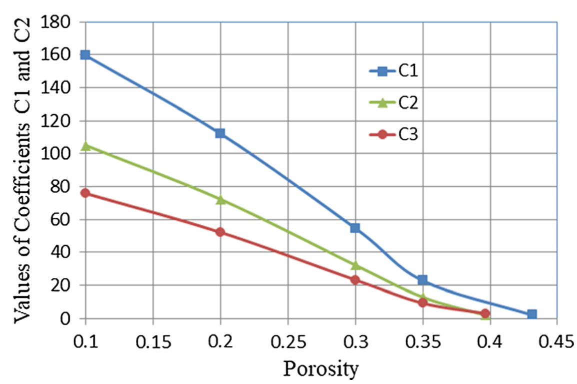

Fig. 14 Coefficients as functions of porosity

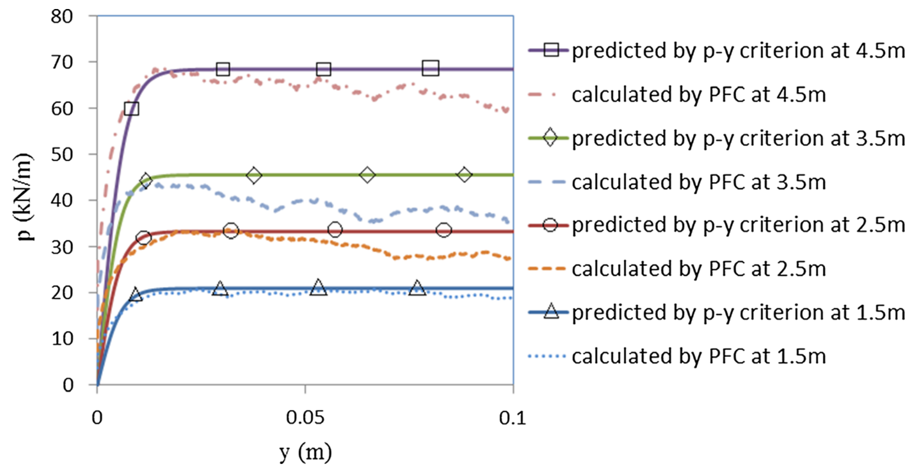

Fig. 15 Comparison of p–y curves predicted by the proposed model with the PFC results

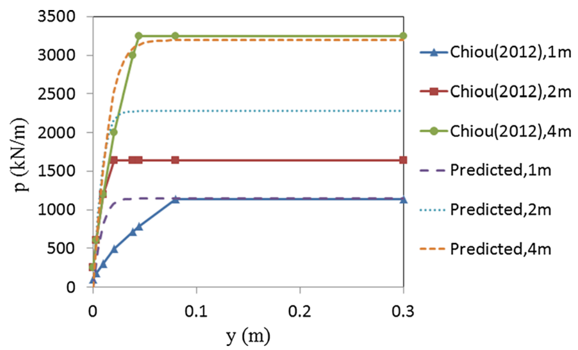

Fig. 16 Comparison of p–y curves predicted by the proposed model with those in Chiou et al. (2012)

For homogeneous gravel (e.g., soil 126), p_u may be computed from the following equation:

$$p_u = \mu \times C_1 \times (D \times \gamma \times H - 2.09). \tag{6}$$

For inhomogeneous gravel (e.g., soil 532) p_u may be computed from the two segmented equations:

$$\text{when } H < 4\text{m}, \quad p_u = \mu \times C_2 \times (D \times \gamma \times H + 1.33), \tag{7}$$

$$\text{when } H \geq 4\text{m}, \quad p_u = \mu \times C_3 \times (D \times \gamma \times H - 7.945), \tag{8}$$

where γ is the effective gravel weight (kN/m^3), and μ is the amplified coefficient for p_u considering the variation of grain size and is defined in Eq. (3b) or Eq. (4b). C_1, C_2, and C_3 are coefficients determined from Fig. 14 as functions of porosity (for example, C_1 is 1.928 when the porosity is 0.43, and C_2 and C_3 are respectively 1.928 and 3.30 when the porosity is 0.40). The curves of the coefficients (shown in Fig. 14) were derived through the analysis of Figs. 5 and 13 considering the variations of pile diameter and gravel weight. In addition, the coefficients need to be slightly adjusted according to the distribution of gravels as shown in Fig. 7.

The p–y curves were evaluated for the pile tests at different depths based on the proposed gravel p–y equations, as depicted in Fig. 15. Note that there is fair agreement between the predicted p–y curves and the calculated p–y values using PFC, particularly at small deflections.

4.2 Comparison of Proposed p–y Equations with Independent Test Data

The lateral load test on the large diameter foundation (5 m in the upper portion and 4 m in the lower portion) of a bridge was carried in situ by Chiou et al. (2012). The results obtained by Chiou et al. were employed as independent testing data to validate the p–y curves obtained from the proposed equations. The test site was located on gravelly soils. The grain-size distribution of the inhomogeneous field gravel was 2/300 mm. The unit weight and the porosity of the gravelly soils were 22.66 kN/m^3 and 31%, respectively, and the calculated porosity was 0.386. The parameter values of C_2 and C_3 were 5.12 and 4.61, respectively.

Figure 16 presents the comparison of proposed p–y curves with the results published by Chiou et al. (2012). The p–y curves from both Chiou et al. (2012)

and the proposed p–y equations demonstrate higher stiffness with the increase of depth in the non-linear section of the curves. The ultimate resistances computed by the proposed p–y equations at depths of 1 and 4 m agree well with the experimental data in Chiou et al. (2012). However, the computed ultimate resistance at a depth of 2 m is slightly higher than that in Chiou et al. (2012). In addition, it can be seen in Fig. 16 that, at depths of 2 and 4 m, there is good agreement between the predicted initial subgrade reactions by the proposed p–y equation and the experimental results in Chiou et al. (2012). Only the predicted initial subgrade reaction at a depth of 1 m is different from that in Chiou et al. (2012). This difference of initial subgrade reaction at a depth of 1 m may be due to the errors based on measurements of the shear wave at the test site, because the equal value of dynamic shear modulus for depth ranges 1–11 m in Chiou et al. (2012) do not satisfy general regularity, such as that shown in relevant literature (Fan and Long 2005) and the triaxial tests for the soil 126 and 532 (Stahl and Konietzky 2011). Moreover, the different analytical methods for predicting the initial modulus seem to be a major reason for the slightly differences. Nonetheless, the p–y approach developed in this study is able to capture the effect of depth on the gravel modulus and the ultimate gravel resistances that match the practical situation reasonably well.

5 Conclusions

This study analyzed the interaction of monopile and gravel under lateral loading at various depths. The goal of this study was ultimately to derive the corresponding p–y model for gravel and account for micromechanical behavior. For this purpose, the three-dimensional discrete particle flow approach was employed for the construction of a model of a single pile in gravelly soil subjected to lateral loads. The modeling of the pile-gravelly soil interaction at different depths was defined using a gravel material layer per unit thickness under the pressure of walls in PFC. In contrast to related methods used in the existing literature, the proposed modeling can easily simulate the realistic mechanical properties of gravelly soil and optimize the computational effort. It is also sufficient for accounting for both the mass of gravel particles and the computational accuracy of lateral resistance. Based on the modeling, the p–y behavior studies for different gravelly soil parameters, types, and depths were implemented. Finally, the general equation of the p–y model for single pile applied to gravelly soil was constructed. The proposed p–y model not only includes the effects of porosity and depths, but also the grain size and different size distributions of gravel.

Acknowledgements This research was supported by the National Natural Science Foundation of China (51579100).

Compliance with Ethical Standards

Conflict of Interest The authors declare that they have no conflict of interest.

References

API (American Petroleum Institute) (2000) Recommended practice for planning, designing, and constructing fixed offshore platforms-working stress design. API Recommended Practice 2A-WSD (RP 2A-WSD), Twenty-first edition, Washington

Azizkandi AS, Baziar MH, Yeznabad AF (2018) 3D dynamic finite element analyses and 1 g shaking table tests on seismic performance of connected and nonconnected piled raft foundations. KSCE J Civ Eng 22(5):1750–1762

Chiou JS, Ko YY, Hsu SY, Tsai YC (2012) Testing and analysis of a laterally loaded bridge caisson foundation in gravel. Soils Found 52(3):562–573

Fan CC, Long JH (2005) Assessment of existing methods for predicting soil response of laterally loaded piles in sand. Comput Geotech 32(4):274–289

Gong J, Liu J (2017) Mechanical transitional behavior of binary mixtures via DEM: effect of differences in contact-type friction coefficients. Comput Geotech 85(5):1–14

Hamed M, Canakci H, Nasr A (2019) Analysis of vertical piles embedded in organic soil under oblique pull-out load. Geotech Test J 42(5):1185–1206

Haque MN, Abu-Farsakh MY (2019) Development of analytical models to estimate the increase in pile capacity with time (pile setup) from soil properties. Acta Geotech 14(3):881–905

Itasca Consulting Group Inc. PFC3D (2008) Particle flow code in 3 dimensions user's guide. Itasca Consulting Group Inc. PFC3D, Minneapolis

Jagodnik V, Arbanas Z (2015) Testing of laterally loaded piles in natural sandy gravels. Int J Phys Model Geotech 15(4):191–208

Jenck O, Dias D, Kastner R (2009) Discrete element modelling of a granular platform supported by piles in soft soil-validation on a small scale model test and comparison to a numerical analysis in a continuum. Comput Geotech 36(6):917–927

Li Q, Yang ZH (2017) P–Y approach for laterally loaded piles in frozen silt. J Geotech Geoenviron Eng 143(5):04017001

Lobo-Guerrero S, Vallejo LE (2007) Influence of pile shape and pile interaction on the crushable behavior of granular materials around driven piles: DEM analyses. Granul Matter 9(3–4):241–250

Macklin PR, Chou NNS (1989) Lateral load test on seven foot diameter caissons. In: Conference name: foundation engineering: current principles and practices, ASCE, New York, pp 1122–1131

Matlock H (1970) Correlations for design of laterally loaded piles in soft clay. In: Proceedings of the annual offshore technology conference, Houston, vol 1970-April, pp 577–594

Mayoral JM, Pestana JM, Seed RB (2016) Multi-directional cyclic p–y curves for soft clays. Ocean Eng 115:1–18

Omidvar M, Iskander M, Bless S (2014) Response of granular media to rapid penetration. Int J Impact Eng 66:60–82

Reese LC (1997) Analysis of laterally loaded piles in weak rock. J Geotech Geoenviron Eng 123(11):1010–1017

Reese LC, Cox WR, Koop FD (1974) Analysis of laterally loaded piles in sand. In: Proceedings, VI annual offshore technology conference, vol II, Houston, pp 473–485

Reese LC, Cox WR, Koop FD (1975) Field testing and analysis of laterally loaded piles in stiff clay. In: Proceedings, VII annual offshore technology conference, vol II, Houston, pp 671–690

Rollins KM, Kwon KH, Gerber TM (2008) Static and dynamic lateral load tests on a pile cap with partial gravel backfill. In: Geotechnical special publication, proceedings of the geotechnical earthquake engineering and soil dynamics IV congress 2008—geotechnical earthquake engineering and soil dynamics, ASCE, GSP 181

Rollins KM, Price JS, Bischoff J (2011) Lateral resistance of piles near vertical MSE abutment walls. In: Proceedings of geo-frontiers 2011: advances in geotechnical engineering. Geotechnical Special Publication, ASCE, no. 211, pp 3526–3535

Rollins K, Price J, Bischoff J (2012) Reduced lateral resistance of abutment piles near MSE walls based on full-scale tests. Int J Geotech Eng 6(2):245–250

Saeedi Azizkandi A, Kashkooli A, Baziar MH (2014) Prediction of uplift pile displacement based on cone penetration tests (CPT). Geotech Geol Eng 32(4):1043–1052

Salimi SN, Yazdanjou V, Hamidi A (2008) Shape and size effects of gravel grains on the shear behavior of sandy soils. In: 10th international symposium on landslides and engineered slopes, Xian, People's Republic of China

Smith TD, Park R, Hannan R (2000) Lateral load prediction and testing of 3.05 m diameter shafts. In: Proceedings of the ASCE geo-institute specialty conference on performance confirmation of constructed geotechnical facilities-performance confirmation of constructed geotechnical facilities, ASCE, GSP 94, 300, pp 184–197

Stahl M, Konietzky H (2011) Discrete element simulation of ballast and gravel under special consideration of grain-shape, grain-size and relative density. Granul Matter 13(4):417–428

Ueda T, Matsushima T, Yamada Y (2011) Effect of particle size ratio and volume fraction on shear strength of binary granular mixture. Granul Matter 13(6):731–742

Vallejo LE (2001) Interpretation of the limits in shear strength in binary granular mixtures. Can Geotech J 38(5):1097–1104

Yu G, Gong W, Chen M et al (2019) Prediction and analysis of behaviour of laterally loaded single piles in improved gravel soil. Int J Civ Eng 17(6):809–822

Zhao H, Zhang J, Qiu P et al (2019) Hierarchical modeling method for DEM simulation and its application in soil-pile-cap interaction and impact case. Int J Geomech 19(7):P04019076